2021 60th IEEE Conference on Decision and Control (CDC)
December 13-15, 2021. Austin, Texas

# Modeling and Adaptive Control of Flexible Quadrotor UAVs

Emre Eraslan[1] and Yildiray Yildiz[2]

*Abstract*— **This paper introduces an analytical framework for the derivation of distributed-parameter equations of motion of a flexible quadrotor. This approach helps obtain rigid and flexible equations of motion simultaneously, in a decoupled form, which facilitates the controller design. An adaptive controller is implemented using the developed model to prevent excessive oscillations due to flexible dynamics and to compensate uncertainties. Furthermore, a delay-dependent stability condition is obtained for the overall system dynamics, including the human UAV operator with reaction time delay, the adaptive controller and the flexible quadrotor dynamics. It is demonstrated via simulations that the flexible arm tip oscillations are reduced when the closed loop reference model adaptive controller is used, compared to a conventional model reference adaptive controller.**

## I. INTRODUCTION

Quadrotor unmanned aerial vehicles (UAVs) are conventionally treated as rigid bodies since most of the time flexible dynamics are negligible. However, for quadrotors that are built using very thin and light materials, flexible dynamics cannot be ignored. The preference of these materials contributes significantly to quadrotor design in terms of i) lower manufacturing and maintenance costs, ii) less battery consumption, iii) less fragility due to collision forces, and iv) less proneness to damages during vertical landing. To be able to conduct a careful analysis for these vehicles, a rigorous mathematical model of flexible dynamics is needed.

Research efforts reported in the open literature pertaining to flexible quadrotor UAVs are relatively scarce. In [1], the flexibility of a quadrotor, upon impact with a wall, is formulated as deformation and reconfiguration of the chassis using a revolute spring and a damper. In [2], a structural vibration analysis of a typical quadrotor UAV chassis using experimental and numerical methods is conducted. to find the lowest vibration regions for electrical equipment placement. In [3], structural resonance is attributed to the interference between the excitation frequencies of the propellers and fundamental frequencies of the UAV structure. It is noted that neither [2] nor [3] contains a dynamical model of the quadrotor UAV that can be employed for control design or analysis of the closed loop control system.

The flexible quadrotor UAV model developed in this paper distinguishes itself from the aforementioned studies by providing a fully distributed dynamical model that can be used for control design. Distributed modeling approach for aerospace applications is not new (see [4] and [5]). These studies are also extended to very flexible fixed-wing UAVs, i.e, that have long flexible arms [6], [7]. However, similar results do not exist for quadrotor UAVs and transferring the existing results to quadrotor UAVs is not a trivial task.

In this paper, we introduce an analytical framework to derive distributed equations of motion of a flexible quadrotor UAV. The applied method is predicated on Lagrangian mechanics using the mean-axes theorem. This approach helps obtain rigid and flexible equations of motion simultaneously, in a decoupled form, which facilitates the controller design. To compensate for uncertainties, we implement two different adaptive controllers: A conventional model reference adaptive controller (MRAC) [8], and a closed loop reference model (CRM) adaptive controller [9]. CRM adaptive controller is developed to reduce the oscillations in MRAC architectures, and its effectiveness is verified experimentally [10]. We demonstrate that CRM adaptive controller indeed helps reduce the vibrations of the flexible quadrotor arms. To the best of authors' knowledge, no similar work exists in the literature, where a distributed modeling of flexible quadrotor UAV is developed together with an adaptive control implementation and a human-in-the-loop stability analysis including reaction time delays. This paper is organized as follows. Section 2 presents the modeling of flexible quadrotor dynamics. The controller design and human-in-the-loop stability analysis are given in Section 3. Simulation results are presented in Section 4.

## II. MODELING OF FLEXIBLE QUADROTOR DYNAMICS

To obtain the distributed equations of motion, we mainly follow the Lagrangian energy based approach presented in [11]. However, unlike [11], our model captures the energy dissipation effects [12] and the flexibility of the quadrotor arms. Below, we first provide the necessary background and then develop the distributed parameter model.

### A. Dynamics of Unconstrained Elastic Bodies

In an unconstrained elastic body, the inertial position $\mathbb{R}_{\mathbb{E}}$ of a mass element $\rho dV$, where $\rho$ is the density and $dV$ is the infinitesimal volume, can be obtained by the summation of its position $\mathbb{R}_{\mathbb{G}}$, relative to a non-inertial body-fixed frame $\mathbb{G}$, and the position $\mathbb{R}_{\mathbb{F}}$ of this body reference frame relative to the inertial frame $\mathbb{F}$ as

$$\mathbb{R}_{\mathbb{E}} = \mathbb{R}_{\mathbb{F}} + \mathbb{R}_{\mathbb{G}}. \tag{1}$$

In the usual rigid body formulation, the time rate of change of $\mathbb{R}_{\mathbb{G}}$ is assumed to be zero [13]. This assumption no longer holds for the flexible body formulation [5]. The position of

[1]Emre Eraslan is with Faculty of Mechanical Science & Engineering, University of Illinois at Urbana-Champaign, Champaign, IL 61820, USA. emree2@illinois.edu

[2]Yildiray Yildiz is with Faculty of Mechanical Engineering, Bilkent University, Bilkent, 06800 Ankara, Turkey. yyildiz@bilkent.edu.tr

the mass element $\rho dV$ relative to the body frame $\mathbb{G}$ can be written as

$$\mathbb{R}_{\mathbb{G}} = \bar{s} + w(\bar{x},t), \tag{2}$$

where $\bar{s}$ is the constant undeformed length, $w(\bar{x},t)$ is the relative flexible displacement and $\bar{x}$ is the generalized coordinate on the body frame. Assuming that free vibration modes of the flexible body are given, the relative displacement $w(\bar{x},t)$ can be expressed in terms of infinitely many mode shapes $W(\bar{x})$ and generalized displacement coordinates $\Upsilon(t)$ as

$$w(\bar{x},t) = \sum_{j=1}^{\infty} W_j(\bar{x})\Upsilon_j(t). \tag{3}$$

Using (3) and applying the mean axes theorem [5], [14], the kinetic energy $\mathbb{T}$ and potential energy $\mathbb{U}$ as in [11] can be expressed as

$$\mathbb{T} = \frac{1}{2}m\frac{d\mathbb{R}_{\mathbb{F}}}{dt}\cdot\frac{d\mathbb{R}_{\mathbb{F}}}{dt} + \frac{1}{2}\omega^T I\omega + \frac{1}{2}\sum_{j=1}^{\infty} M_j\dot{\Upsilon}_j^2(t), \tag{4}$$

$$\mathbb{U} = -mg\mathbb{R}_{\mathbb{F}} + \frac{1}{2}\sum_{j=1}^{\infty}\bar{\omega}_j^2 M_j\Upsilon_j^2(t), \tag{5}$$

where the term $M_j$ is the generalized mass term and $\bar{\omega}_j$ is the natural frequency corresponding to the $j^{\text{th}}$ flexible degree of freedom.

### *B. Equations of Motion for an flexible Quadrotor UAV*

The flexible quadrotor UAV consists of three different types of masses, that is, the main body mass $m_b$, the arm mass $m_c$ and the rotor mass $m_r$, all of which add up to the total mass $m = m_b + 4m_c + 4m_r$. The position variable vector and the Euler angles vector pertaining to the center of mass in the body frame are expressed as $\xi = [x,y,z]^T \in \mathbb{R}^3$ and $\upsilon = [\phi,\theta,\psi]^T \in \mathbb{R}^3$, respectively. The inertial angular velocity vector of the center of mass is given by $\omega = [p,q,r]^T \in \mathbb{R}^3$. The rotation matrix $R^B \in \mathbb{R}^{3\times3}$ that transforms the vectors from $\mathbb{G}$ to $\mathbb{F}$ is the $(\psi,\theta,\phi)$ sequence. The thrust force on the $k^{\text{th}}$ rotor is given by

$$F_k = k_t\Omega_k^2, \tag{6}$$

where $k_t$ is the thrust factor and $\Omega_k$ is the angular velocity of the $k^{\text{th}}$ rotor. The total thrust force $F_b$ represented in the body frame $\mathbb{G}$ is

$$F_b = \sum_{k=1}^{4} k_t\Omega_k^2 e_3, \tag{7}$$

where $e_3$ is the corresponding unit vector. $F_b$ represented in the inertial frame $\mathbb{F}$ is given as

$$\mathbb{Q}_\xi = R^B F_b. \tag{8}$$

Denoting the torques developed due to the rotational velocities of the rotors as $\tau_b$, we can further define the gyroscopic torques are given as

$$\tau_g = -J_r[\dot{\upsilon}\times e_3]\Omega_g, \tag{9}$$

where $J_r$ is the moment of inertia of the rotor and $\Omega_g$ is the gyroscopic velocity. The total torque, $\mathbb{Q}_\upsilon$, represented in the inertial frame $\mathbb{F}$ is obtained as

$$\mathbb{Q}_\upsilon = \tau_b + \tau_g. \tag{10}$$

The control input vector, $u$, is taken as

$$u = R^{\Omega_s}\Omega_s, \tag{11}$$

where $R^{\Omega_s}$ is the corresponding constant transformation matrix, and $\Omega_s = [\Omega_1^2,\Omega_2^2,\Omega_3^2,\Omega_4^2]^T$. It follows from (11) that

$$u = k_t^{-1}R^{\Omega_s}F, \tag{12}$$

where $F$ is the force vector. The generalized coordinates for the flexible body dynamics is given as $q = [\xi^T,\upsilon^T,\Upsilon_j^T]^T \in \mathbb{R}^{(p+6)}$, $j = 1,2,\ldots,p$, where $p$ is the number of flexible degrees of freedom, which is infinite in theory but can be truncated to a finite number depending on the level of modeling fidelity. The relation between the rotational velocity vector $\omega$ and time rate of change of the Euler angles vector are expressed as

$$\omega = R^\upsilon\dot{\upsilon}, \tag{13}$$

where $R^\upsilon$ is the corresponding transformation matrix. Substituting (13) into (4), it follows that

$$\mathbb{T}(q,\dot{q}) = \frac{1}{2}m\frac{d\mathbb{R}_{\mathbb{F}}}{dt}\cdot\frac{d\mathbb{R}_{\mathbb{F}}}{dt} + \frac{1}{2}\dot{\upsilon}^T R^{\upsilon^T} I R^\upsilon\dot{\upsilon} + \frac{1}{2}\sum_{j=1}^{\infty} M_j\dot{\Upsilon}_j^2(t). \tag{14}$$

The Lagrangian consisting of the set of generalized coordinates for the flexible quadrotor UAV can be expressed as

$$\mathbb{L}(q,\dot{q}) = \mathbb{T} - \mathbb{U}. \tag{15}$$

The friction term is added exogenously to the formulation in terms of a Rayleigh dissipation function [12] as

$$\mathbb{D}(\dot{q}) = \frac{1}{2}\sum_{j=1}^{\infty}\sigma_c\dot{\Upsilon}_j^2(t), \tag{16}$$

where the term $\sigma_c$ is the damping coefficient term. The Lagrangian equation is then given as

$$\frac{d}{dt}\left(\frac{\partial\mathbb{L}}{\partial\dot{q}_i}\right) - \left(\frac{\partial\mathbb{L}}{\partial q_i}\right) + \left(\frac{\partial\mathbb{D}}{\partial\dot{q}_i}\right) = \mathbb{Q}_i, \tag{17}$$

where $i = 1,2,\ldots,(p+6)$, and $Q_i$ is the generalized force. Using (14)-(17), we obtain the rigid part of the equations of motions identical to those of a rigid quadrotor UAV [15] and the flexible part as

$$M_j\ddot{\Upsilon}_j(t) + \sigma_c\dot{\Upsilon}_j(t) + \bar{\omega}_j^2 M_j\Upsilon_j(t) = \mathbb{Q}_{\Upsilon_j}(t). \tag{18}$$

### *C. Transverse Vibrations of flexible Arms*

The resulting equations of motion for the flexible part (18) are of a relatively simple form, although it is not clear yet what the terms $M_j,\sigma_c,\bar{\omega}_j$ and $\mathbb{Q}_{\Upsilon_j}(t)$ represent in the overall system. In the literature, aeroelastic behavior of flexible aircraft is interpreted as the motion of morphing wings. Upon considering the flexibility of the quadrotor, the arms can be modeled as thin cantilever beams undergoing transverse

vibrations owing to continuous motion and agile maneuvers of the quadrotor.

Although a large body of research is devoted to the modeling of undamped Euler-Bernoulli beams under various boundary conditions, relatively small amount of studies can be found for beams with damping: The damping is formulated as an internal property using the viscoelastic Kelvin-Voigt model by [16]. On the other hand, a model of a cantilever beam with external damping is developed where a dashpot is attached at the free end [17]. For simplicity, we use the latter approach and write the equations of motion governing the damped beam as

$$E_c J_c \frac{\partial^4 w(\bar{x},t)}{\partial \bar{x}^4} + \rho_c A_c \frac{\partial^2 w(\bar{x},t)}{\partial t^2} + \sigma_c \frac{\partial w(\bar{x},t)}{\partial t} = F(\bar{x},t), \quad (19)$$

where $E_c$ and $J_c$ are the Young's modulus and moment of inertia of the beam, respectively, $\rho_c$ is the density, $A_c$ is the cross-sectional area, $\sigma_c$ is the damping coefficient of the beam and $F(\bar{x},t)$ is the concentrated thrust force acting at the beam edge. The solution to the homogeneous part of this equation can be obtained by using (3). The boundary conditions can be stated as

$$W(0) = 0, \quad (20)$$

$$\frac{dW(0)}{d\bar{x}} = 0, \quad (21)$$

$$E_c J_c \frac{d^2 W(L_c)}{d^2 \bar{x}} = 0, \quad (22)$$

$$E_c J_c \frac{\partial^3 w(L_c,t)}{\partial^3 \bar{x}} = m_r \frac{\partial^2 w(L_c,t)}{\partial^2 t}. \quad (23)$$

Taking $F(\bar{x},t) = 0$, substituting (3) into (19), and solving it together with (20)-(23), the transcendental frequency equation [18] is obtained as

$$1 + \frac{1}{\cos\bar{\beta}_j \cosh\bar{\beta}_j} - \bar{m}\bar{\beta}_j(\tan\bar{\beta}_j - \tanh\bar{\beta}_j) = 0, \quad (24)$$

where $\bar{\beta}_j = \beta_j L_c$ is the solution of (24) and, $\beta_j = \sqrt[4]{\frac{\rho_c A_c \bar{\omega}_j^2}{E_c J_c}}$ is a specific constant obtained from the separation of (19) corresponding to the $j^{\text{th}}$ natural frequency $\bar{\omega}_j$, and $\bar{m} = m_r/m_c$ denotes the ratio of the rotor mass $m_r$ to the mass of the cantilever beam $m_c$. For a given $j^{\text{th}}$ mode, we can solve for $\bar{\beta}_j$ in (24) and calculate a corresponding natural frequency $\bar{\omega}_j$. Following this procedure, we also obtain the mode shape $W_j(\bar{x})$, which can be written as

$$W_j(\bar{x}) = \bar{\gamma}_j \left[(\cos\beta_j\bar{x} - \cosh\beta_j\bar{x}) - \bar{\beta}_j^* (\sin\beta_j\bar{x} - \sinh\beta_j\bar{x})\right], \quad (25)$$

where $\bar{\gamma}_j$ is a normalization constant corresponding to the $j^{\text{th}}$ mode and $\bar{\beta}_j^*$ is a term related to boundary conditions. To solve for generalized displacement coordinates $\Upsilon_j(t)$ in (18), we apply orthogonality conditions and obtain that

$$\ddot{\Upsilon}_j(t) + \sigma_c'\dot{\Upsilon}_j(t) + \bar{\omega}_j^2\Upsilon_j(t) = \int_0^{L_c} W_j(\bar{x})F(\bar{x},t)d\bar{x}, \quad (26)$$

where $\sigma_c' = \sigma_c/(\rho_c A_c)$. It is noted that there is a one-to-one correspondence between (18) and (26). The generalized mass term $M_j$ in (18) refers to $\rho_c A_c$, which is the mass per unit length. Considering the right hand side of (26) and recalling that $F_k(\bar{x},t) = F_k(t)\delta(\bar{x} - L_c)$ is a concentrated thrust force for the $k^{\text{th}}$ quadrotor arm, $k = \{1,2,3,4\}$, where $\delta(\bar{x})$ is the Dirac's delta function, it can be shown that

$$\int_0^{L_c} W_j(\bar{x})F_k(t)\delta(\bar{x} - L_c)d\bar{x} = W_j(L_c)F_k(t). \quad (27)$$

Substituting (27) into (26), we obtain that

$$\ddot{\Upsilon}_{kj}(t) + \sigma_c'\dot{\Upsilon}_{kj}(t) + \bar{\omega}_{kj}^2\Upsilon_{kj}(t) = W_j(L_c)F_k(t), \quad j = 1,2,..,\infty. \quad (28)$$

For each arm of the quadrotor, (28) has infinitely many solutions corresponding to each $\bar{\omega}_j$. We choose to take the first three natural frequency values, that is, the variable $j$ takes the values of 1, 2 and 3. The relative displacement $w_k(\bar{x},t)$ of the arm $k$ at the tip can then be calculated as

$$w_k(L_c,t) = \sum_{j=1}^{3} W_j(L_c)\Upsilon_{kj}(t). \quad (29)$$

Using (29), we define the corresponding flexible states $z_{kj}$, $k = \{1,2,3,4\}$, $j = \{1,2,3\}$, as

$$z_{kj}(t) = W_j(L_c)\Upsilon_{kj}(t), \quad (30)$$

Multiplying (28) with $W_j(L_c)$ and using (30), (28) can be rewritten as

$$\ddot{z}_{kj}(t) + \sigma_c'\dot{z}_{kj}(t) + \bar{\omega}_{kj}^2 z_{kj}(t) = W_j^2(L_c)F_k(t). \quad (31)$$

This implies that the tip oscillations at each arm $k$ can be modeled as the summation of solutions of three mass spring damper systems with the same damping coefficient $\sigma_c'$ but different spring constants $\bar{\omega}_{kj}^2$. Therefore, the flexible states for arm $k$ can be written in a state space form as

$$\dot{z}_e^k = A_e' z_e^k + B_{ze}' F_k, \quad (32)$$

where $z_e^k = [z_{k1},\ \dot{z}_{k1},\ z_{k2},\ \dot{z}_{k2},\ z_{k3},\ \dot{z}_{k3}]^T$, $A_e'$ and $B_{ze}'$ are the corresponding matrices. Finally, concatenating all the four arms under the same state space representation, introducing an actuator effectiveness matrix $\Lambda$, and substituting (12) into (32), it is obtained that

$$\dot{z}_e = A_e z_e + B_e \Lambda u. \quad (33)$$

where $A_e$ and $B_e$ are the corresponding matrices.

## III. Controller Design and Human-in-the-Loop Stability Analysis

The overall closed loop control system consisting of an inner and an outer loop is presented in Fig. 1. The inner loop constitutes the uncertain flexible quadrotor dynamics with a closed loop reference model (CRM) adaptive controller. The human operator exists in the outer loop, where s/he observes the commanded and actual plant states, and produces a reference input for the inner loop.

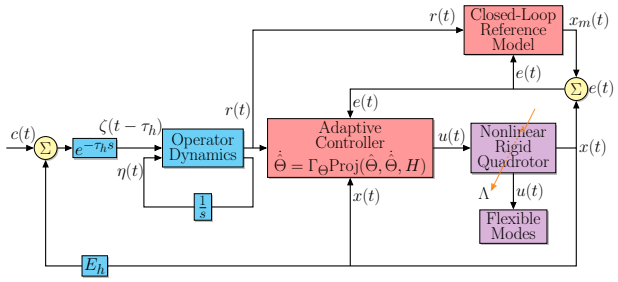


Fig. 1: Block diagram of the overall control architecture including the operator dynamics.

### A. Controller Design

The rigid part of the equations of motion are linearized around a hover position by using small angle approximations. The resulting equations of motion can be represented as

$$\begin{aligned} \dot{x}_p(t) &= A_p x_p(t) + B_p \Lambda u(t) + B_p \Theta_p^T \Phi_p(x_p(t)) \\ y_p(t) &= C_p x_p(t), \end{aligned} \tag{34}$$

where $x_p \in \mathbb{R}^{n_p}$ comprises the position and the Euler angles variables and their corresponding derivatives, $u \in \mathbb{R}^{n_m}$ is the control input, $\Theta_p \in \mathbb{R}^{n_s \times n_m}$ is an unknown weight matrix, $\Phi_p : \mathbb{R}^{n_p} \to \mathbb{R}^{n_s}$ is a known vector of the form $\Phi_p(x_p) = [\Phi_{p_1}(x_p), \Phi_{p_2}(x_p), \cdots, \Phi_{p_s}(x_p)]^T$ of high order nonlinear effects and $y_p \in \mathbb{R}^{n_r}$ is the plant output. Besides, $A_p \in \mathbb{R}^{n_p \times n_p}$ is constant and unknown, $B_p \in \mathbb{R}^{n_p \times n_m}$ is a known constant matrix, with the assumption that $(A_p, B_p)$ is controllable. The control goal of interest is bounded command tracking in the presence of uncertainties, that is, tracking a reference $r(t) \in \mathbb{R}^{n_r}$ produced by the human pilot (See Fig. 1). To achieve tracking, a new state vector $e_p \in \mathbb{R}^{n_r}$ is defined as the integral of the tracking error,

$$e_p(t) = \int_0^t [y_p(\varepsilon) - r(\varepsilon)] d\varepsilon, \tag{35}$$

and augmented with (34), which results in the dynamics

$$\dot{x}(t) = Ax(t) + B\Lambda u(t) + B\Theta_p^T \Phi_p(x_p(t)) + B_m r(t), \tag{36}$$

where $A$, $B$ and $B_m$ are the corresponding matrices and $x(t) = [x_p(t)^T, e_p(t)^T]^T \in \mathbb{R}^{(n_p+n_m)}$ is the augmented state vector with $n = n_p + n_m$. The control law is determined as

$$u(t) = u_{\text{bl}}(t) + u_{\text{ad}}(t), \tag{37}$$

where $u_{\text{bl}}(t) \in \mathbb{R}^{n_m}$ and $u_{\text{ad}}(t) \in \mathbb{R}^{n_m}$ are the baseline and the adaptive control laws, respectively. The baseline controller is given as

$$u_{\text{bl}}(t) = -K^T x(t), \tag{38}$$

where $K \in \mathbb{R}^{n \times n_m}$ is a fixed state feedback control gain matrix. We choose this gain such that

$$A_m = A - B\Lambda K^T \tag{39}$$

becomes a stable matrix. The reference model is selected as

$$\dot{x}_m(t) = A_m x_m(t) + B_m r(t) - Le(t), \tag{40}$$

where $x_m \in \mathbb{R}^n$ is the reference model state vector, $e(t) = x(t) - x_m(t)$ is the tracking error and $L \in \mathbb{R}^{n \times n} < 0$ is a constant matrix such that $(A_m + L)$ is Hurwitz. Substituting (37), (38) and (39) into (36), one obtains

$$\dot{x}(t) = A_m x(t) + B_m r(t) + B\Lambda[u_{\text{ad}}(t) + \Theta^T \Phi(x(t))], \tag{41}$$

where $\Theta^T = \left[\Lambda^{-1}\Theta_p^T\right] \in \mathbb{R}^{n_m \times n_s}$ is the unknown overall weight matrix and $\Phi^T(x(t)) = \left[\Phi_p^T(x_p(t))\right] \in \mathbb{R}^{(n_s+n)}$ is a vector of high order nonlinear effects. We choose an adaptive control of the form

$$u_{\text{ad}}(t) = -\hat{\Theta}^T \Phi(x(t)), \tag{42}$$

where $\hat{\Theta} \in \mathbb{R}^{(n_s+n) \times n_m}$ is the matrix of time-varying adaptive parameters. The adaptive law is given by

$$\dot{\hat{\Theta}} = \Gamma_\Theta \Phi(x(t)) e^T(t) PB, \tag{43}$$

where $\Gamma_\Theta \in \mathbb{R}^{[(n_s+n)\times n_m] \times [(n_s+n)\times n_m]}$ is a diagonal positive definite matrix of adaptive gains and $P \in \mathbb{R}^{n \times n}$ is the unique symmetric positive definite solution of the Lyapunov equation

$$(A_m + L)^T P + P(A_m + L) = -Q, \tag{44}$$

where $Q \in \mathbb{R}^{n \times n} > 0$ is a positive definite symmetric matrix. To prevent adaptive parameter drifts, in other words, to ensure that the time-varying adaptive parameters are bounded, the projection algorithm [19] is employed as

$$\dot{\hat{\Theta}} = \Gamma_\Theta \,\text{Proj}(\hat{\Theta}, \Phi(\text{x(t)})\text{e}^{\text{T}}(\text{t})\text{PB}, \text{H}), \tag{45}$$

where $\text{Proj}(\Theta, \text{Y}, \text{H})$ is the projection operator and $H$ is a vector of convex functions. Defining the adaptive parameter estimation error as $\tilde{\Theta} = \hat{\Theta} - \Theta$, and subtracting (40) from (41), the reference model tracking error is obtained as

$$\dot{e}(t) = A_m e(t) - B\Lambda\tilde{\Theta}^T \Phi(x(t)) + Le(t). \tag{46}$$

Using the Lyapunov function candidate

$$\mathbb{V}(e, \tilde{\Theta}) = e^T(t) P e(t) + \text{tr}[(\tilde{\Theta}^T \Gamma^{-1} \tilde{\Theta})\Lambda], \tag{47}$$

it can be shown that

$$\dot{\mathbb{V}}(e(t), \tilde{\Theta}(t)) = -e^{\text{T}}(t)\,\text{Pe}(t) \leq 0. \tag{48}$$

This implies that the equilibrium point of (43) and (46) is stable. The convergence of $e$ to zero can be shown using Barbalat's Lemma. However, here the lemma is inapplicable, since $\dot{\mathbb{V}}(e(t), \tilde{\Theta}(t))$ cannot be proven to be bounded, yet. The term $x(t) = e(t) + x_m(t)$ contains the reference model state $x_m(t)$, which can grow unboundedly due to the reference $r(t)$ produced by the human pilot model. For this reason, the dynamics of the outer loop needs to be investigated to determine whether or not $x_m(t)$ and $r(t)$ are bounded.

### B. Outer Loop Dynamics

We use a linear model with a time delay for human operator dynamics, represented as

$$\dot{\eta}(t) = A_h \eta(t) + B_h \zeta(t-\tau_h), \tag{49}$$
$$r(t) = C_h \eta(t) + D_h \zeta(t-\tau_h), \tag{50}$$

where $\eta(t) \in \mathbb{R}^{n_\eta}$ is the human state vector, $\tau_h \in \mathbb{R}^+$ is the reaction delay, and $A_h \in \mathbb{R}^{n_\eta \times n_\eta}, B_h \in \mathbb{R}^{n_\eta \times n_c}, C_h \in \mathbb{R}^{n_r \times n_\eta}$, and $D_h \in \mathbb{R}^{n_r \times n_c}$ are constant matrices. $r(t) \in \mathbb{R}^{n_r}$ is the reference formed by the human operator (see Fig. 1). The input to the human dynamics is the feedback error term

$$\zeta(t) = c(t) - E_h x(t), \tag{51}$$

where $E_h \in \mathbb{R}^{n_c \times n}$ is a constant matrix that allows to choose a subset of the state $x(t)$ as feedback. The analysis in this chapter follows the similar steps used in [20]. Using (50) and (51), (40) and (49) can be rewritten compactly as a single delay equation as

$$\dot{\mu}(t) = \mathbb{A}_n \mu(t) + \mathbb{A}_d \mu(t-\tau_h) + \Pi(\cdot), \tag{52}$$

where $\mu(t) \triangleq \left[x_m^T(t), \eta^T(t)\right]^T$, $\mathbb{A}_n$, $\mathbb{A}_d$, and $\Pi(\cdot)$ are the corresponding matrices. Since $e(t)$ is shown to be bounded in the previous section and the command $c(t)$ is bounded, the matrix $\Pi(\cdot)$ is bounded. A delay-dependent stability result for the overall dynamics is given in the theorem below, which can be used to determine the stability regions.

*Theorem 3.1:* Consider the dynamics given in (52). If the real parts of all the infinitely many roots of the equation

$$\det\left(sI - \left(\mathbb{A}_n + \mathbb{A}_d e^{-\tau_h s}\right)\right) = 0 \tag{53}$$

have strictly negative real parts, then $\mu(t) \in \mathbb{L}_\infty$ and $\lim_{t\to\infty} e(t) = 0$. (See [20] for the proof.)

## IV. Simulations

In this section, we first explain the simulation scenario with the controller design and the stability limits of the operator dynamics, and then discuss the simulation results.

### A. Simulation Scenario

In the simulations, the rigid part of the equations of motion and (33) are used as the plant model. The human operator is assumed to behave like a proportional integral (PI) controller, with a reaction time delay. This model is consistent with the operator model introduced in (49)-(51), and can be represented as

$$G_{\mathrm{PI}}(s) = K_p \frac{T_p s + 1}{s} e^{-\tau_h s}, \tag{54}$$

where $K_p > 0$ and $T_p > 0$ are model constants, and $\tau_h$ is the human operator reaction time delay.

Two anomalies are injected at $t_a = 16s$, which result in loss of control effectiveness of 75% and 50% in the second and third rotors, respectively.

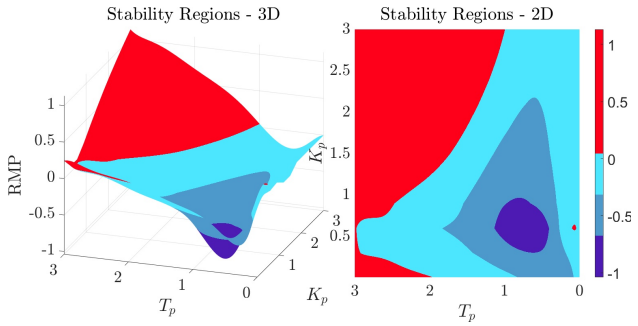


Fig. 2: Variation of rightmost pole location with respect to simultaneous change in $K_p$ and/or $T_p$.

### B. Stability Limits

As stated in Theorem 3.1, once the CRM adaptive controller is designed as given in (37)-(45), the stability of the overall system is determined by the roots of the characteristic polynomial presented in (53). We use the DDE-BIFTOOL [21] to find the rightmost root, among infinitely many of them, of this polynomial for the simulation example. Fig. 2 shows the location of the rightmost root of the characteristic polynomial (53) for different values of $K_p$ and $T_p$. The red areas in the figure represent the unstable regions. It can be argued that the system can be swept into the unstable region for moderately high values of $T_p$.

### C. Simulation Results

Tracking performances of three different closed loop control systems are presented in Fig. 3. In the figure, the autonomous flights using a model reference adaptive controller and a closed loop reference model adaptive controller are labeled as MRAC, and CRM, respectively. Human operator controlled flight, where a CRM is used as the controller (See Fig. 1) is labeled as CRM-H. For coherence, all closed loop control systems are color-coded, that is, MRAC with blue, CRM with red and CRM-H with green. Fig. 4 shows that CRM induces smoother trajectory responses and control inputs. The effect of human operator involvement is also observed as delayed responses to commanded inputs, due to human reaction lag. As expected, CRM based controllers provide better tracking performances.

It should also be ascertained whether or not control input excitations are close to the natural frequencies of the flexible modes. The natural frequencies, $\bar{\omega}_{kj}$, $k = \{1,2,3,4\}$, $j = \{1,2,3\}$, of the first three flexible modes of four quadrotor arms (see (31)) are calculated as 131 rad/s, 1365 rad/s and 1865 rad/s, respectively. Fig. 4 demonstrates that none of the controllers excite these frequencies. On the other hand, it is shown in Fig. 5 that the arm tips oscillate with lower frequencies and amplitudes in CRM based configurations. This is also observed in quadrotor trajectories provided in Fig. 3.


## Acknowledgment

This research was sponsored by the Scientific and Technological Research Council of Turkey under Grant 118E937.

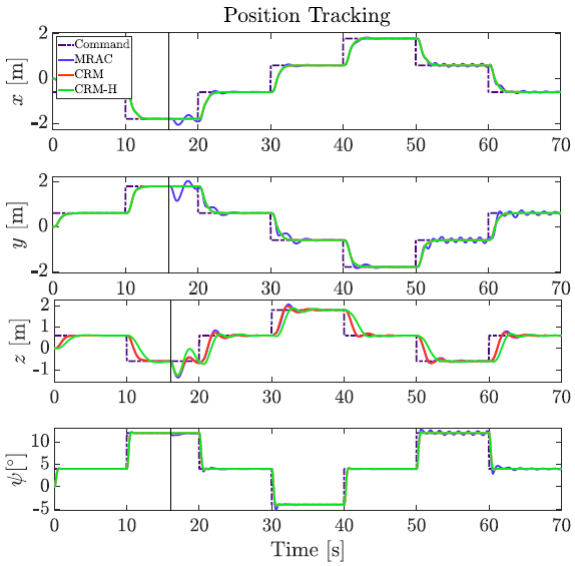


Fig. 3: The position tracking performance of the MRAC, CRM and CRM-H configurations.

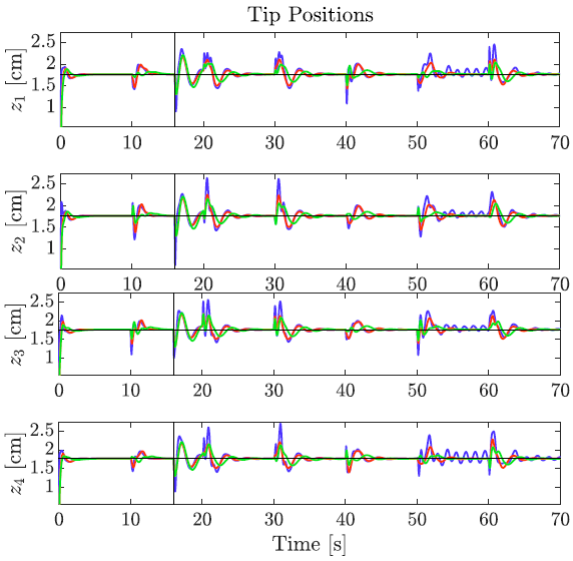


Fig. 5: The arm tip oscillations of the MRAC (blue), CRM (red) and CRM-H (green) configurations.

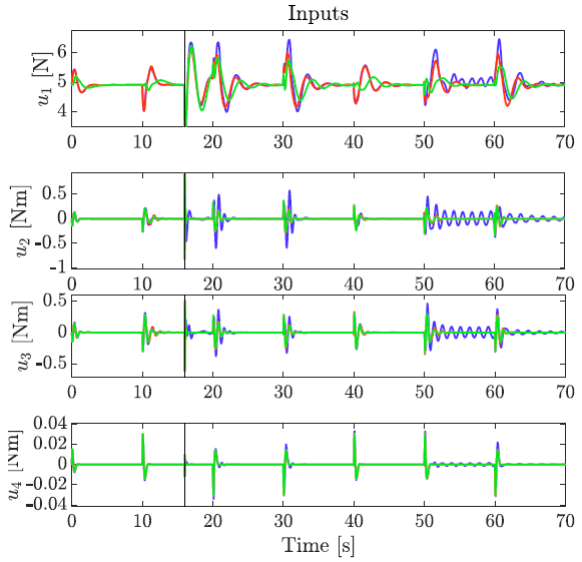


Fig. 4: The control inputs of the MRAC (blue), CRM (red) and CRM-H (green) configurations.

## REFERENCES


[1] M. Srikanth, A. Annaswamy, and E. . Lavretsky *Dynamic modeling and control of a flexible four-rotor UAV. In AIAA Guidance, Navigation, and Control Conference*, vol. 8050, 2010.

[2] J. Verbeke and S. Debruyne, "Vibration analysis of a uav multirotor frame," in *Proceedings of ISMA 2016 International Conference on Noise and Vibration Engineering*, pp. 2401–2409, 2016.

[3] A. Tullu, Y. Byun, J. N. Kim, and B. S. Kang, "Parameter optimization to avoid propeller-induced structural resonance of quadrotor type unmanned aerial vehicle," *Composite Structures*, vol. 193, pp. 63–72, 2018.

[4] L. Meirovitch and H. D. Nelson, "On the high-spin motion of a satellite containing elastic parts," *Journal of Spacecraft and Rockets*, vol. 3, no. 11, pp. 1597–1602, 1966.

[5] M. R. Waszak and D. K. Schmidt, "Flight dynamics of aeroelastic vehicles," *Journal of Aircraft*, vol. 25, no. 6, pp. 563–571, 1988.

[6] M. C. Van Schoor and A. H. von Flotow, "Aeroelastic characteristics of a highly flexible aircraft," *Journal of Aircraft*, vol. 27, no. 10, pp. 901–908, 1990.

[7] M. Ritter, J. Jones, and C. E. Cesnik, "Enhanced modal approach for free-flight nonlinear aeroelastic simulation of very flexible aircraft," *In*, vol. 15, 2016.

[8] K. S. Narendra and A. M. Annaswamy, *Stable adaptive systems*. Courier Corporation, 2012.

[9] T. Yucelen, G. De La Torre, and E. Johnson *N. Improving transient performance of adaptive control architectures using frequency-limited system error dynamics*, vol. 87, no. 11, pp. 2383–2397, 2014.

[10] E. Eraslan, Y. Yildiz, and A. M. Annaswamy, "Shared control between pilots and autopilots: Illustration of a cyber-physical human system," *IEEE Control Systems Magazine*, vol. 40, no. 6, pp. 79–99, 2020.

[11] M. R. Waszak, J. B. Davidson, and D. K. Schmidt, "A simulation study of the flight dynamics of elastic aircraft," *Volume*, vol. 1, 1987.

[12] R. Vepa, *Flight Dynamics, Simulation, and Control: For Rigid and Flexible Aircraft*. CRC Press, 2014.

[13] R. F. Stengel, *Flight dynamics*. Princeton University Press, 2015.

[14] H. Hesse, R. Palacios, and J. Murua, "Consistent structural linearization in flexible aircraft dynamics with large rigid-body motion," *AIAA journal*, vol. 52, no. 3, pp. 528–538, 2014.

[15] S. Bouabdallah, *Design and control of quadrotors with application to autonomous flying (No*. THESIS). Epfl, 2007.

[16] S. N. Mahmoodi, S. E. Khadem, and M. Kokabi, "Non-linear free vibrations of kelvin–voigt visco-elastic beams," *International Journal of Mechanical Sciences*, vol. 49, no. 6, pp. 722–732, 2007.

[17] M. Gürgöze and H. Erol, "Dynamic response of a viscously damped cantilever with a viscous end condition," *Journal of Sound and Vibration*, vol. 298, no. 1-2, pp. 132–153, 2006.

[18] S. S. Rao, *Vibration of continuous systems (Vol. 464)*. New York: Wiley, 2007.

[19] S. S. Tohidi, Y. Yildiz, and I. Kolmanovsky, "Adaptive control allocation for constrained systems," *Automatica*, vol. 121, no. 2020, pp. 5–1098, 2020.

[20] T. Yucelen, Y. Yildiz, R. Sipahi, E. Yousefi, and N. Nguyen, "Stability limit of human-in-the-loop model reference adaptive control architectures," *International Journal of Control*, vol. 91, no. 10, pp. 2314–2331, 2018.

[21] K. Engelborghs, T. Luzyanina, and D. Roose, "Numerical bifurcation analysis of delay differential equations using dde-biftool. acm transactions on mathematical software (toms)," vol. 28, no. 1, pp. 1–21, 2002.